Published online 7 April 2022

Nucleic Acids Research, 2022, Vol. 50, No. 7 ***4187–4196***
https://doi.org/10.1093/nar/gkac232

Formation of non-base-pairing DNA microgels using directed phase transition of amphiphilic monomers

Chanseok Lee[1,†], Sungho Do[2,†], Jae Young Lee[1], Minju Kim[3], Sang Moon Kim[3], Yongdae Shin[1,2,4,*] and Do-Nyun Kim[1,2,5,*]

[1]Institute of Advanced Machines and Design, Seoul National University, Seoul 08826, Korea, [2]Department of Mechanical Engineering, Seoul National University, Seoul 08826, Korea, [3]Department of Mechanical Engineering, Incheon National University, Incheon 22012, Korea, [4]Interdisciplinary Program in Bioengineering, Seoul National University, Seoul 08826, Korea and [5]Institute of Engineering Research, Seoul National University, Seoul 08826, Korea

Received January 04, 2022; Revised February 27, 2022; Editorial Decision March 23, 2022; Accepted March 26, 2022

ABSTRACT

Programmability of DNA sequences enables the formation of synthetic DNA nanostructures and their macromolecular assemblies such as DNA hydrogels. The base pair-level interaction of DNA is a foundational and powerful mechanism to build DNA structures at the nanoscale; however, its temperature sensitivity and weak interaction force remain a barrier for the facile and scalable assembly of DNA structures toward higher-order structures. We conducted this study to provide an alternative, non-base-pairing approach to connect nanoscale DNA units to yield micrometer-sized gels based on the sequential phase transition of amphiphilic unit structures. Strong electrostatic interactions between DNA nanostructures and polyelectrolyte spermines led to the formation of giant phase-separated aggregates of monomer units. Gelation could be initiated by the addition of NaCl, which weakened the electrostatic DNA-spermine interaction while attractive interactions between cholesterols created stable networks by crosslinking DNA monomers. In contrast to the conventional DNA gelation techniques, our system used solid aggregates as a precursor for DNA microgels. Therefore, *in situ* gelation could be achieved by depositing aggregates on the desired substrate and subsequently initiating a phase transition. Our approach can expand the utility and functionality of DNA hydrogels by using more complex nucleic acid assemblies as unit structures and combining the technique with top-down microfabrication methods.

INTRODUCTION

DNA has attracted attention as a suitable building material for nanostructures owing to its sequence-specific binding characteristics (1). By utilizing the cooperative self-assembly of sequence-programmed DNA strands, we can fabricate nanostructures with a wide range of sizes and geometries, from small-scale DNA junctions (2) to complex 2D and 3D shapes (3–5). To date, scaling up of DNA assemblies to micro and even larger scales remains a major challenge for structural DNA nanotechnology (6,7). Conventional approaches have used weak interactions between DNA, such as base-pairing of short complementary sequences and blunt-end stacking, resulting in successive formation of hierarchically assembled DNA superstructures (8), lattice-packed crystals (9,10), and hydrogels (11–22).

Among them, DNA hydrogels typically comprise a network of branched small DNAs (11,16–20) or long strands synthesized from the rolling circle amplification (21,22), and they have been widely used for intracellular delivery units (15) and other biological applications (19). Generally, base pairing-driven assembly can be used as a powerful tool for formation of DNA hydrogels by designing the length and sequence of connecting regions. However, it usually requires a temperature gradient or precise manipulation of elevated temperatures throughout the self-assembly process to initiate and modulate the transient states of DNA hybridization (23,24). Additionally, careful consideration of the dimensions and mechanical flexibility of monomer units is required because such parameters significantly influence the formation of gel networks and their mechanical properties (12,16).

Considering diverse dimensions, shapes, and functions of DNA nanostructures, a non-base-pairing interaction can be an attractive mechanism for constructing higher-order DNA assemblies (25–27). Electrostatic interaction is one of

*To whom correspondence should be addressed. Email: dnkim@snu.ac.kr
Correspondence may also be addressed to Yongdae Shin. Email: ydshin@snu.ac.kr
†These authors contributed equally to the work.

the most appealing forces to bind DNA assemblies since DNA has strong negative charges associated with its phosphate backbone (28,29). When mixed with polycations such as spermidine, spermine, and poly-l-lysine (PLL) peptide, phase separation of DNA strands into large-scale solid precipitates occurs (28,30,31). Recent studies have revealed that the phase characteristics of DNA-polycation condensates can be controlled by adding NaCl, since the monovalent cation Na^+ neutralizes the surface charge of DNA and weakens the electrostatic interaction between DNA and polycations (29,32). However, since higher-order structures are assembled solely via electrostatic attraction, they are sensitive to external ionic conditions. Thus, a robust binding mechanism is required to create and maintain their macromolecular assemblies to provide a stable interaction between monomers.

We conducted this study to utilize spermine-induced phase separation of amphiphilic DNA nanostructures to realize the on-demand formation of non-base-pairing DNA microgels with controllable size and viscosity. The structural connection between DNA monomers is facilitated by cholesterol-cholesterol interactions. This is an ideal mechanism to realize the phase-transition-based gelation technique as cholesterol can be easily attached to DNA nanostructures via triethylene glycol (TEG) linkers. Further, the addition of NaCl effectively triggered the reconfiguration of aggregated monomers into networked gel structures. The increased ion concentration stimulates cholesterol connections by enhancing hydrophobic interactions (33,34) while the mobility of monomers increases by weakening the electrostatic interaction between DNA and spermine. In contrast to the conventional base-pairing-based gelation methods in which the gel is made from a dispersed or liquid-like state, our method provides a phase transition from solid to gel at ambient temperature. By utilizing this characteristic, the *in situ* gelation of aggregates was demonstrated by depositing solid aggregates on micropatterned surfaces with different geometries.

MATERIALS AND METHODS

Materials

All DNA strands were purchased from Bioneer Corporation (www.bioneer.co.kr, Korea). DNA strands decorated with cholesteryl-TEG or fluorophore (Cy5) were purified using HPLC; otherwise Bio-RP purification was used. Sequences of all DNA strands are summarized in Supplementary Tables S1 and S2. All DNA strands were diluted to 100 μM using deionized (DI) water. DNA concentration was measured using a microvolume UV-VIS spectrophotometer (NanoDrop One; Thermo Fisher Scientific, USA). Spermine and other reagents were purchased from Sigma–Aldrich (USA).

DNA self-assembly and sample preparation

Equimolar amounts of four DNA strands were mixed to construct 4-arm DNA units with a final concentration of 12 μM. One of the strands was replaced with one attached to Cy5 at a molecular ratio of 1:99 for confocal microscopy. Thermal annealing was performed using a thermocycler (T100; Bio-Rad, USA). A mixture of all DNA strands with 100 mM NaCl was heated to 80°C for 5 min, and it was slowly cooled from 80°C to 25°C at −1°C per 20 min. DNA-spermine conjugates were prepared by mixing annealed DNA nanostructures and 4 mM spermine solution in a 1:1 volumetric ratio, and the solution was vortexed more than ten times using a microvolume pipette. The mixed solution was then incubated at 25°C for at least 30 min. For the formation of DNA microgel, 3× NaCl buffer solution was subsequently added to the DNA-spermine solution to reach 1× target salt concentration at the final state. To make smaller microgels, vortexing was performed by pipetting and mixing the whole solution more than ten times using a microvolume pipette.

Polyacrylamide gel electrophoresis (PAGE)

Polyacrylamide gel was cast by mixing 6 mL of 40% acrylamide/bis-acrylamide solution (19:1 ratio), 400 μL of 50× Tris-Acetate-EDTA (TAE) buffer, 13.6 μL of DI water, 120 μL of 10% (w/v) ammonium persulfate solution, and 12 μL of tetramethylethylenediamine (TEMED). Gels were mounted on a Mini-Protean Tetra Cell (Bio-Rad) filled with 1× TAE buffer, and 1 μL of each sample mixed with gel loading dye purple (B7024S, New England BioLabs) was loaded onto the gel. After running the gels at 100 V for 70 min, they were stained with SYBR gold solution for 10 min. Gel imaging was performed using a Gel Doc XR+ documentation system (Bio-Rad).

Confocal microscopy measurements

Differential interference contrast (DIC) and fluorescence microscopy were performed using an Eclipse Ti2 inverted microscope (Nikon, Japan) with a 647 nm laser. Approximately 30 μL of the incubated sample was dropped onto a confocal plate, sealed with the lid of the plate, and incubated in a temperature chamber. After approximately 20 min of incubation until a sufficient amount of condensates were visible, images were taken at 40× magnification and 1024 × 1024 pixel resolution. For time-lapse imaging, a 512 × 512 pixel resolution was typically used. The stage and chamber temperature was maintained at 25°C throughout the experiment. Calibration of raw images and merging of DIC and fluorescent images were performed using imageJ2 software (https://imagej.net/ImageJ2).

DNA fraction in solution measurements

The sample (50 μL) was centrifuged at 21000 g using a benchtop centrifuge (1730R, LaboGene, Korea) for 10 min, maintaining the temperature at 25°C. Twenty microliters of the supernatant was carefully obtained from the top of the solution, and the DNA density was measured using NanoDrop.

Fabrication of micropatterned surfaces

Micropatterned surfaces with UV-curable material were fabricated from silicon master mold via UV replication (35). The silicon master molds engraved with hole and groove arrays were fabricated using conventional photolithography

and reactive ion etching. The surface of silicon master was treated with octafluorocyclobutane (C_4F_8) gas in an inductively coupled plasma chamber for an easy detachment of cured polymers. Following this, a UV-curable PUA prepolymer (PUA MINS 311 RM; Changsung sheet, Korea) was prepared to construct the micropatterned surfaces. A drop of PUA was dispensed onto the silicon mold, and a 145 μm-thick coverslip (Deckglaser; Duran, Germany) was slightly pressed against the liquid drop to be used as a supporting layer. The precursor was exposed to UV light (Fusion Cure System, Minuta Tech, Korea) for 60 s, and the cured patterns were detached from the mold. The patterns were then exposed to UV light for 3 h to fully cure the prepolymer residue remaining on the surface.

MD simulation

Initial connectivity and sequences of the 4-arm DNA unit were designed using caDNAno (36) (Supplementary Table S4), and its all-atom representation was constructed using SNUPI (37) by inducing a high electrostatic force deliberately. The atomic force field parameters of cholesteryl-TEG and spermine molecules were calculated using the CHARMM General Force Field (38) and CHARMM-GUI (39) webserver. An improved nonbonding force field was employed for amine−carboxylate and amine−phosphate interactions (40). VMD (41) was used for preparation of the simulation system and visualization. The initial system comprised four regular or amphiphilic DNA units, which were solvated and ionized at a concentration of 100 mM Na^+.

NAMD (42) was used for MD simulation. The molecular systems were minimized using the conjugate gradient method for 10,000 steps to remove steric clashes. After minimization, the systems were simulated for 500 ns each at a constant pressure of 1 bar and temperature of 300 K in the NPT ensemble using the Nosé-Hoover Langevin piston (43) and Langevin thermostat (42). Additionally, all simulations were performed with cubic periodic boundary conditions, the CHARMM36 force field (44), and an improved parameterization for ions (40,45) using multiple time-stepping of 2–4–12 fs, SETTLE algorithm for rigid water molecules (46), RATTLE algorithm to rigidly maintain all other covalent bonds involving hydrogen atoms (47), and 8–10–12 Å cutoff for van der Waals, short-range electrostatic forces, and long-range electrostatic interactions using the particle mesh Ewald method (48) with a 1.0 Å resolution grid. The detailed simulation system is summarized in Supplementary Table S5.

RESULT AND DISCUSSION

Non-base-pairing gelation of DNA nanostructures was mediated via a two-step phase transition utilizing electrostatic and hydrophobic interactions (Figure 1). For demonstration, a 4-arm junction structure with 20-bp-long arms was designed as a regular unit structure. Here, base-pairing interactions between regular units are not allowed (Figure 1A). An amphiphilic DNA unit has more than one cholesterol at the end of the arm connected to a TEG linker (49,50). Here, two cholesterols were diagonally attached at the end of the arms (Figure 1B). By mixing polyelectrolyte spermine with DNA units, strong electrostatic interactions between DNA and spermine drive the formation of solid precipitates of DNA units from the dispersed phase. As the charge ratio of amines and phosphates in the solution (N/P ratio) is an important factor for DNA condensation (29), we sought the optimal N/P ratio using a 20-bp-long dsDNA strand (Supplementary Figure S1). It was confirmed that DNA-spermine aggregates were sufficiently formed with an N/P ratio exceeding 4; therefore, the N/P ratio was ranged from 6.9 to 8.3 throughout the experiment. On addition of spermine, aggregation of monomers was observed for both the regular and amphiphilic monomers. However, a distinct difference was observed when NaCl was added to the DNA-spermine mixture. Since Na^+ ions attached near the DNA strands neutralize the negative surface charges, weak interactions between DNA nanostructures and spermine molecules resulted in the re-dispersion of aggregates (Figure 1A, right) (28). On the contrary, in case of the amphiphilic unit, cholesterol-cholesterol interactions play a major role in connecting neighboring monomers and forming microscale gel condensates (Figure 1B, right).

We designed amphiphilic 4-arm monomer units and investigated the optimal conditions for an effective two-step phase transition (from dispersed phase to solid aggregates and then from solid phase to gels) in terms of the unit design and cation types and concentrations. Four different designs, blunt-ended (BL), 8-mer thymine single-stranded DNA (ssDNA) overhang (SS), regular cholesterol (CH), and weak cholesterol (wCH), could be applied at the end of each arm (Figure 2A). The wCH design was introduced to reduce the hydrophobic interactions between cholesterols by placing the SS moiety at the opposite end of cholesterol. It was reported that the hydrophobic base region of ssDNA is wrapped around cholesterol, resulting in a decreased interaction between cholesterols (49). We created nine structural variations in 4-arm junction structures by changing the type and number of cholesterols, and all designs were successfully self-assembled via thermal annealing in a solution containing 100 mM NaCl (Figure 2B, Materials and Methods, and Supplementary Table S3).

We first investigated the phase transition behavior of amphiphilic DNA units with regular cholesterols and blunt-ends ('CH-BL' designs) (Figure 2C and Supplementary Figure S2). Regardless of the number of cholesterols in monomers, solid precipitates were formed when the structures were mixed with spermine (Figure 2C, second column). However, on addition of NaCl to the DNA-spermine mixture, the final states of condensates were highly different depending on the number of cholesterols in each unit. When a single cholesterol was attached (termed 1CH-3BL), no notable condensates were observed when the final NaCl concentration exceeded 100 mM. However, as the number of cholesterols increased to two (2CH-2BL) and three (3CH-1BL), gelation of aggregates was clearly observed as their morphologies became rounded. With full cholesterol density (4CH), the condensates failed to form rounded geometries regardless of the final NaCl concentration. Additionally, condensates of amphiphilic monomers tended to form more solid-like shapes at 900 mM NaCl concentration, indicating that excessive monovalent ions may have induced

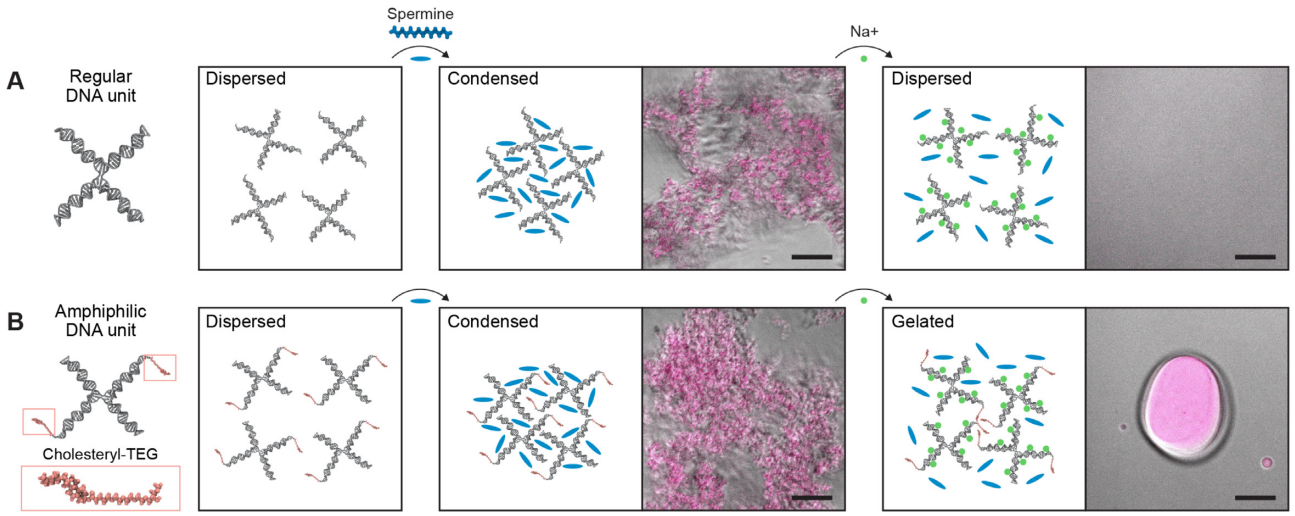

Figure 1. Schematic illustration of the DNA gelation process using phase transition behavior. (**A**) Regular DNA units were condensed with the addition of spermine via electrostatic interaction. When Na+ ions were added, a weakened DNA-spermine interaction led to the dissolution of the aggregates. Scale bars: 20 μm. (**B**) Amphiphilic DNA units having cholesteryl-TEG at the end of arms have a similar condensation behavior with regular units. However, the cholesterol–cholesterol interaction maintains the connection between monomers, leading to the formation of microgels with the addition of Na+ ions. Scale bars: 20 μm.

strong hydrophobic interactions, which could prevent the relaxation of gels into smooth boundaries (Supplementary Figure S2).

Amphiphilic DNA units with weak cholesterols and ssDNAs ('wCH-SS' designs) were characterized by the same salt concentrations (Figure 2D). Interestingly, we observed highly spherical high-order assemblies, reminiscent of liquid-like droplets, when the 1wCH-3SS design was mixed with spermine at a final NaCl concentration of 50 mM (Figure 2D and Supplementary Figure S3). This phenomenon correlates with the previous observation that the interaction between spermine and single-stranded DNA can result in liquid-liquid phase separation (51). The fluorescence-recovery-after-photobleaching (FRAP) test revealed that the droplets had a liquid-like property as the fluorescent signal significantly recovered after bleaching, albeit not fully (green dots and line in Figure 2E and Supplementary Figure S4). The structure with two weak cholesterols (2wCH-2SS) failed to form microgels at an NaCl concentration of 300 mM, indicating a decreased hydrophobic interaction as compared to that of the 2CH-2BL design. The 3wCH-1SS design showed ideal gelation behavior since microgels with very smooth boundaries were formed within an NaCl concentration range of 300-500 mM. In FRAP measurements, DNA microgels consisting of 3wCH-1SS showed a slightly higher recovery rate than 2CH-2BL gels (violet and pink dots and lines in Figure 2E). This indicates that the modulation of cholesterol moiety can enable fine control over the condensation characteristics and viscosity of microgels. To confirm that the observed effects originated from the SS overhang attached near the cholesterol, we tested other designs where SS overhangs were not attached near cholesterol (Supplementary Figure S5). They showed very similar gelation behaviors with blunt-ended designs. This indicated that only one ss-DNA overhang near cholesterol showed a notable effect on the formation and characteristics of DNA microgels.

The phase diagram for CH-BL and wCH-SS units over a range of NaCl concentrations showed that weakened cholesterols contributed to the formation of microgels with reduced amounts of salt (Figure 2F). The common range of NaCl required for gelation was 300–500 mM for 2CH-2BL, 3CH-1BL, and 3wCH-1SS structures; however, the viscosity of the gels, assessed from the shape and FRAP measurements, differed depending on the unit design. The amount of gelated monomers was estimated by measuring the fraction of DNA in solution after gelation and centrifugation (Figure 2G and Materials and Methods). As the number of cholesterols increased, more condensates formed in the solid or gel phase. In the 3wCH-1SS case with 300 mM NaCl, approximately 72% of the total DNA formed gel structures.

To determine whether the type of polyamine affected the condensation and gelation behavior of the amphiphilic DNA units, spermidine and PLL with a chain length range of 30–70 K were used (Figure 3A). In contrast to spermine, which successfully formed solid aggregates with a wide range of concentrations, spermidine failed to form visible aggregates within the N/P range of 1.3 to 13 (Figure 3A, second column). PLL showed sensitive aggregation behavior with respect to the N/P ratio. Analysis of the N/P effect for regular and amphiphilic dsDNA showed that an N/P ratio near 1 could facilitate the formation of large-scale aggregates (Supplementary Figure S6). The aggregation behavior of 3wCH-1SS unit was also similar (Figure 3A). Gelation of DNA-PLL aggregates was tested using 3wCH-1SS units and PLL with different chain lengths (1–5 K, 4–15 K, and 30–70 K) (Figure 3B). At the same NaCl concentration, the 1–5 K PLL mixture transited into relatively smaller microgels whereas the 4–15 K and 30–70 K PLL mixtures showed

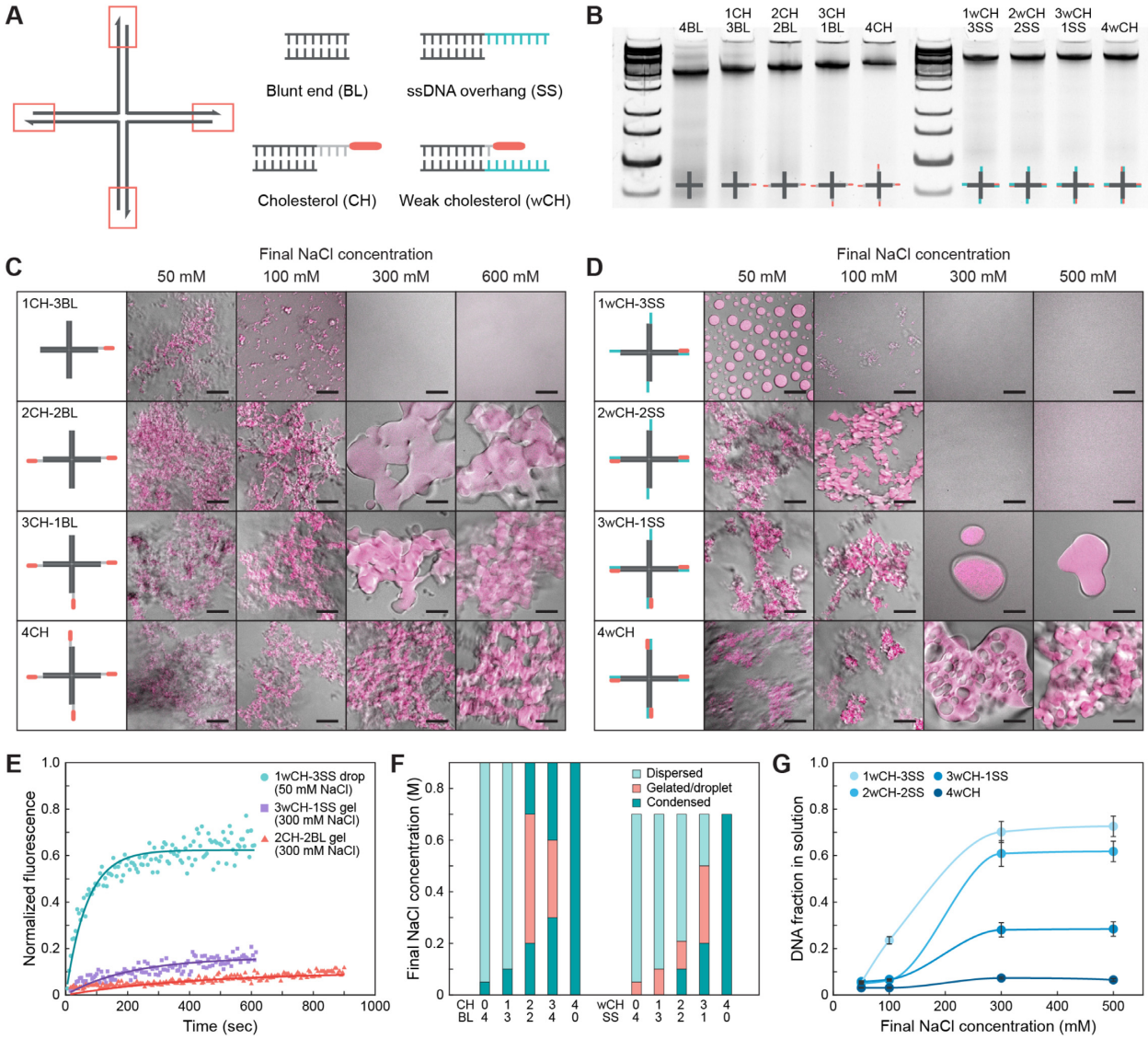

Figure 2. Design of amphiphilic 4-arm units and their phase transition characteristics with spermine. (**A**) Schematic illustration of the 4-arm monomer unit design. Arrowheads indicate the 3' ends of DNA strands. Orange boxes at the end of each arm indicate modifiable regions. Detailed illustrations of four different end-of-arm designs are shown. Green-colored ssDNA refers to 8-mer poly-T overhang. Refer to Supplementary Table S1 for sequences of the strands and Supplementary Table S3 for the selection of strands for each structure. (**B**) PAGE of self-assembled regular and amphiphilic 4-arm DNA units having blunt-end (BL) and regular cholesterol (CH) moieties and weak cholesterol (wCH) and single-stranded overhang (SS) moieties. Ladder: TriDyeTM Ultra Low Range DNA Ladder (New England BioLabs). (**C**) Final states of the monomer units having CH and BL arms. Refer to Supplementary Figure S2 for more variation of NaCl concentration. Scale bars: 30 μm. (**D**) Final states of the monomer units having wCH and SS arms. Scale bars: 30 μm. (**E**) FRAP results of selective cases shown in (**C**) and (**D**) (green: 1wCH-3SS with 50 mM NaCl, violet: 3wCH-1SS with 300 mM NaCl, red: 2CH-2BL with 300 mM NaCl). Refer to Supplementary Figure S4 for confocal microscope images. (**F**) Phase diagram for various DNA unit-spermine complexes with varying NaCl concentrations. Increasing the number of cholesterols delays or hinders the formation of microgels. (**G**) Fraction of DNA in the solution of 16 cases shown in (**D**).

solid-like behaviors (Figure 3B and Supplementary Figure S7). This indicated that the interaction between DNA and long PLL chains was too strong to effectively form gelated structures.

An important aspect of phase-transition-based gelation technique is that the initial formation of DNA-spermine complex in the solid phase is critical for the formation of DNA microgels. When spermine and NaCl were simultaneously mixed with amphiphilic DNA monomer units, almost no microgels were formed (Figure 3C). This indicated that the assembly process of DNA microgel was dependent on the pathway since the precipitation of monomer units accompanying an increased concentration of cholesterol moieties is a critical condition for active cholesterol-cholesterol interaction (52). With increased NaCl concentrations, the electrostatic attraction between DNA-spermine was not sufficient to gather DNA monomers, resulting in failure to form microgels. In the absence of spermine, high concentration of NaCl (1 M) could induce the formation of gel-like grains for 2CH-2BL structures (Supplementary Figure S8).

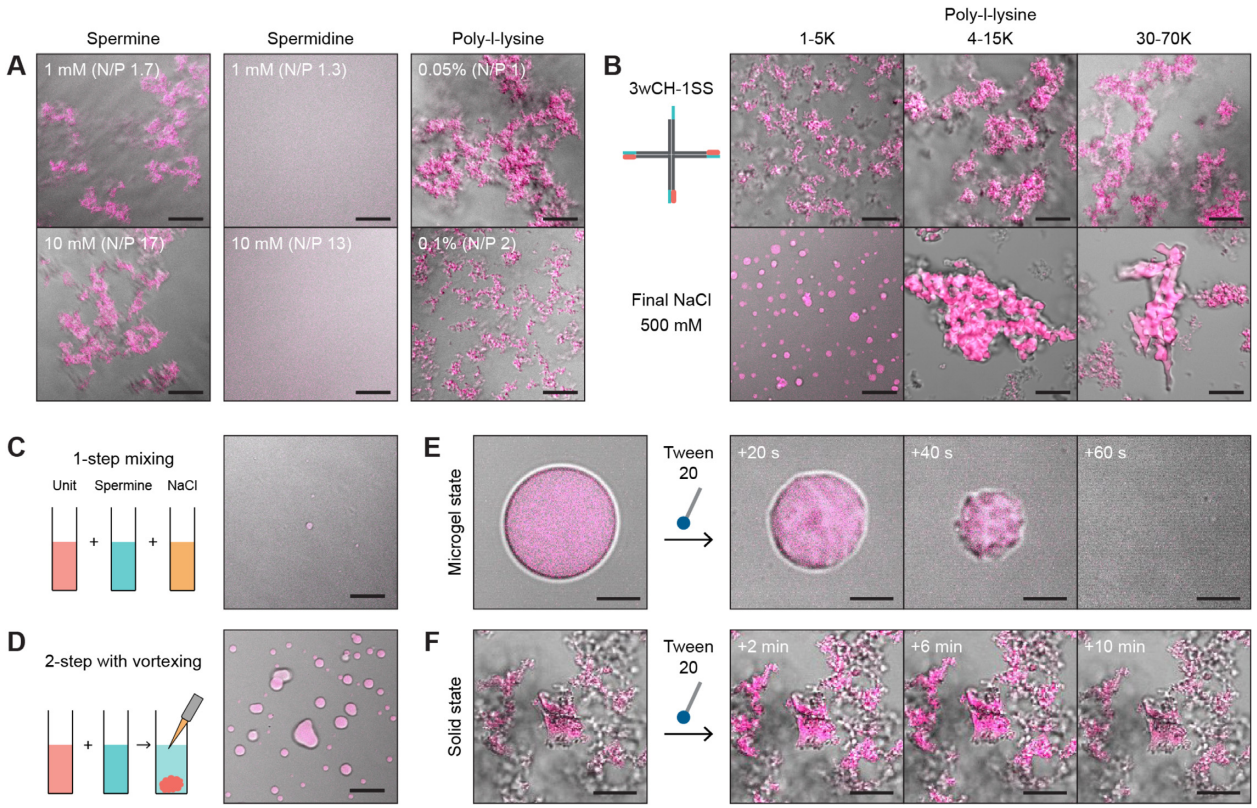

Figure 3. Counter ion-dependent phase transition behavior and other characteristics of amphiphilic DNA microgels. (**A**) Comparison of the aggregation behavior of 3wCH-1SS unit with spermidine, spermine, and 30-70K poly-l-lysine with different N/P ratios. (**B**) Gelation of 3wCH-1SS and poly-l-lysine mixture with the addition of NaCl. Refer to Supplementary Figure S7 for additional results. (**C**) Phase characteristics of the case where 3wCH-1SS units, spermine, and NaCl were simultaneously mixed. Only few aggregates with small sizes were shown when the final NaCl concentration was 300 mM. Scale bar: 20 μm. (**D**) Same composition as (C), but 3wCH-1SS units and spermine were mixed first, and following this, NaCl was added with vortexing using a micropipette. Several microgels with reduced sizes were observed. Refer to Supplementary Figure S9 for size distribution. Scale bar: 20 μm. (**E**) Surfactant Tween 20 was added to the 3wCH-1SS microgel, leading to complete dissolution of the gel within a minute. Images were shown with a 20 s interval after the addition of Tween 20. Refer to Supplementary Figure S10 for the dissolution images for another case. Scale bars: 10 μm. (**F**) When Tween 20 was added to 3wCH-1SS aggregates before gelation, their shapes were unchanged since electrostatic interactions between DNA-spermine were unaffected by Tween 20. Refer to Supplementary Figure S11 for the wide-field images. Scale bars: 20 μm.

However, their shapes were highly irregular, indicating that gelation process was incomplete.

It should also be noted that the final sizes of DNA microgels were determined by the initial size of solid aggregates. When NaCl solution was slowly added to the DNA-spermine mixture while avoiding disassembly of aggregates, large DNA microgels whose contact areas with the substrate were typically larger than 1000 μm^2 were fabricated; additionally, even larger gels were available when the concentration of monomer units was increased. In contrast, the size of microgels was significantly reduced when the mixture solution was vortexed using a micropipette (Materials and Methods). Approximately 90% of the 3wCH-1SS microgels were formed with a contact area of less than 40 μm^2 (Figure 3D and Supplementary Figure S9). This also implies that the size of DNA microgels can be facially controlled by manipulating the size of solid aggregates.

To verify that the hydrophobic interaction between cholesterols is a dominant driving force for maintaining DNA microgels, nonionic surfactant polysorbate 20 (Tween 20) was added to the solution. As the hydrophobic tail of Tween 20 molecules interacts with cholesterols and weakens the cholesterol-cholesterol interaction, disassembly of DNA microgels is expected. Indeed, 3wCH-1SS microgels rapidly dissolved after the addition of 10% Tween 20 solution with a 25% volumetric ratio (Figure 3E and Supplementary Figure S10). In sharp contrast, dispensing the same amount of Tween 20 in the solution containing DNA-spermine aggregates did not induce any significant change in their shape and phase characteristics (Figure 3F and Supplementary Figure S11). This observation strongly indicated that the dominant mechanism constituting DNA microgels was the cholesterol-cholesterol interaction between monomers whereas electrostatic interactions were the driving force in DNA-spermine aggregates before gelation.

One of the major advantages of our two-step isothermal gelation process is that gel structures can be made on a desired substrate *in situ* by slowly dispensing NaCl solution onto the substrate where DNA-spermine aggregates are placed (Figure 4A). In our experiment, the 3wCH-1SS design was selected owing to its faster gelation time (20-30 min) than the 2CH-2BL design (>30 min, Supplementary Figure S12) with a smaller viscosity. For further demonstration, *in situ* gelation was performed on the micropat-

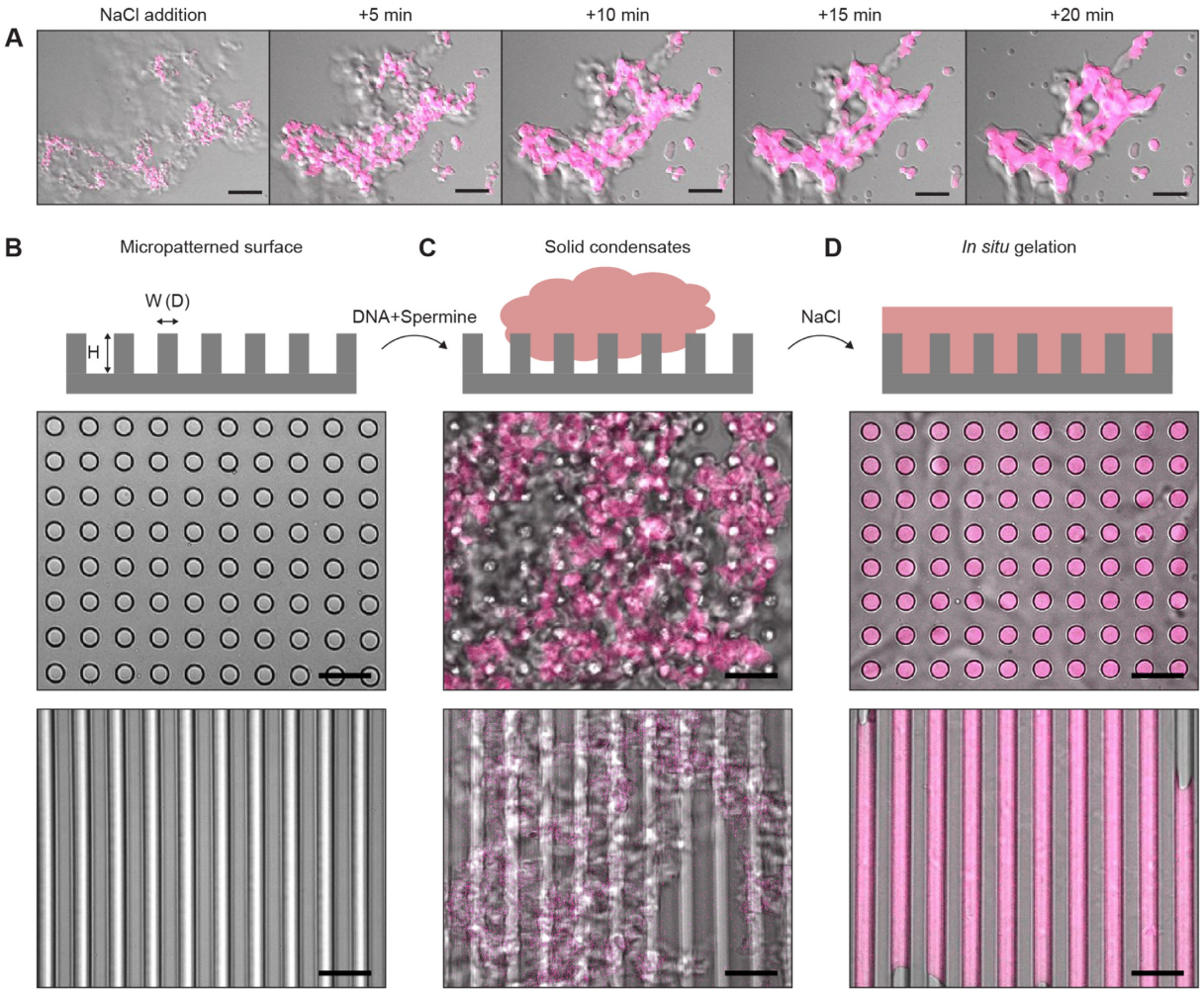

Figure 4. In situ gelation of amphiphilic DNA condensates. (**A**) Time-lapse images of gelation of 3wCH-1SS aggregates. NaCl solution (800 mM) was deposited on the substrate to make the final NaCl concentration to 300 mM. Scale bars: 50 μm. (B-D) Demonstration of in situ gelation on micropatterned surfaces. Hole pattern: D = 10 μm H = 5 μm. Groove pattern: W = 10 μmH = 25 μm. (**C**) 3wCH-1SS aggregates were dropped onto the substrates. (**D**) Gelation of condensates by dispensing NaCl solution onto the substrate. Refer to Supplementary Figure S13 for images during phase transition and Supplementary Figure S14 for wide-field images. Scale bars in (**B-D**): 30 μm.

terned surfaces (Figure 4B-4D and Supplementary Figures S13 and S14). Micropatterned surfaces were fabricated via replica molding using a UV-curable material on an MEMS-fabricated silicon substrate. (Figure 4B and Materials and Methods). We used a hole pattern (diameter of 10 μm and depth of 5 μm) and groove pattern (width of 10 μm and depth of 25 μm). A mixture containing 3wCH-1SS aggregates with spermine was deposited on the micropatterned surfaces (Figure 4C). On addition of NaCl to the sample, solid aggregates on the substrate were gradually transformed into microgels, filling in the engraved regions of micropatterns (Figure 4D and Supplementary Figures S13 and S14). In addition to previous approaches such as UV-triggered reaction (53,54) and site-directed growth (55), our distinctive method based on solid to gel transition offers a simple and effective approach for rapid formation of microscale DNA gels with surface-confined geometries.

To understand the mechanism of gelation and interaction between DNA units, MD simulations were performed (Figure 5 and Supplementary Figures S15-S17). Four regular (without cholesterols) or amphiphilic (two cholesterols were diagonally attached) monomers were placed in a water box containing spermine with an N/P ratio of 4 and Na^+ concentration of approximately 200 mM (Materials and methods). Regular and amphiphilic DNA units showed different binding behaviors and corresponding fluctuation characteristics. While regular units remained in a monomeric state throughout the simulation, amphiphilic monomers were connected via cholesterol–cholesterol interactions (Figure 5A and B, and Supplementary Figures S16 and S17). Time-lapse snapshots of the simulated system showed that cholesterol connections were made within 100 ns, and they were maintained thereafter (Supplementary Figure S17). These results were consistent with the experimental observation that dispersed and gel states were observed with 4BL and 2CH-2BL designs with similar ionic concentrations, respectively (Figure 2C). For quantitative comparison, the root-mean-square fluctuation (RMSF) magnitudes of all DNA bases comprising each monomer were calculated (56) (Figure 5C). Decreased RMSF values in DNA bases near

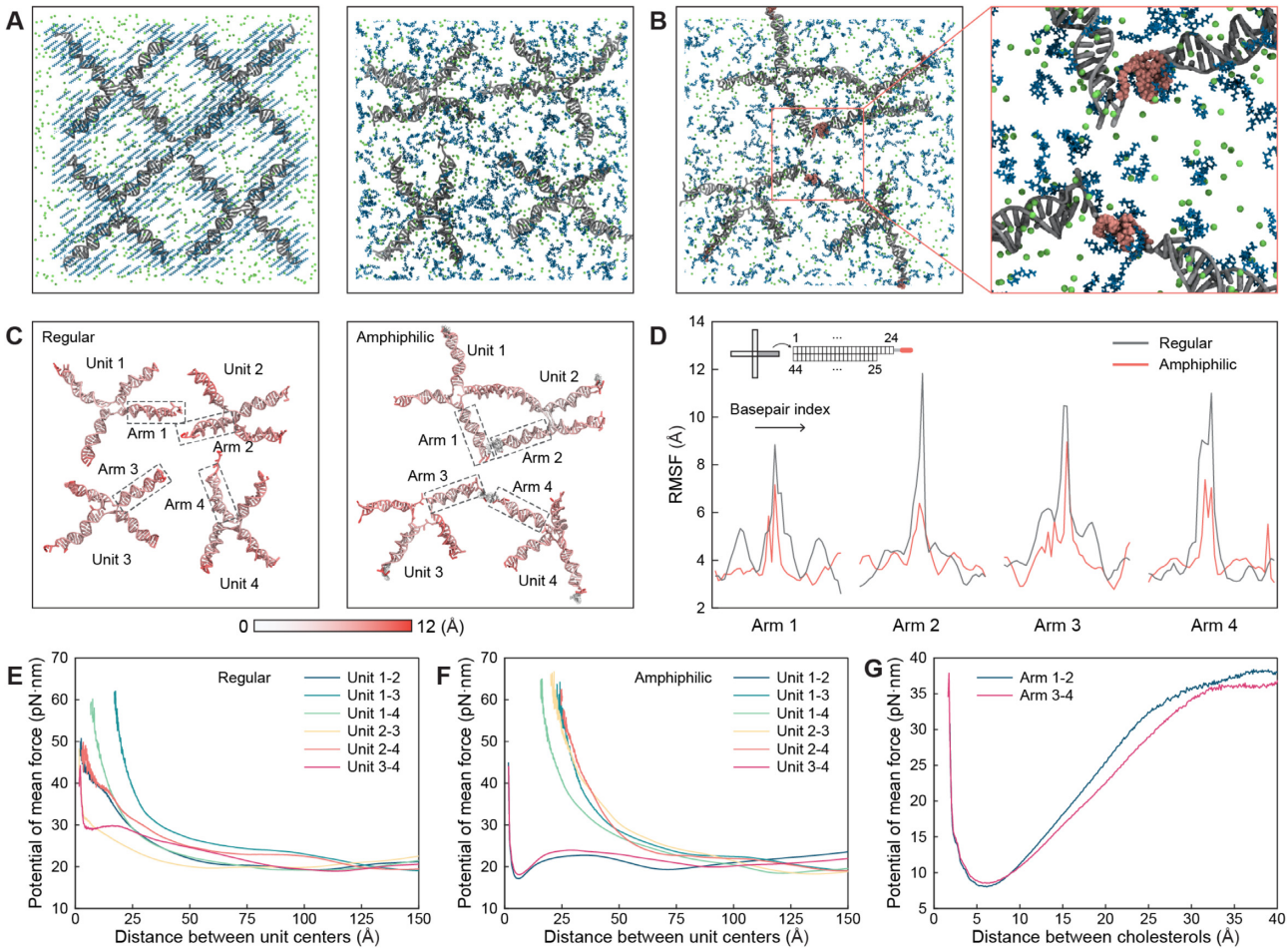

Figure 5. Molecular dynamics simulation of regular and amphiphilic DNA units. (**A**) Initial and final configuration of regular DNA units. Green spheres indicate Na+ ions and blue molecules represent spermine ions. Refer to Supplementary Figure S16 for more snapshots. (**B**) Final configuration of amphiphilic DNA units. The orange box is an enlarged view of the connection region. Red-colored molecules are cholesteryl-TEG. Refer to Supplementary Figure S17 for more snapshots. (**C**) Root-mean-square fluctuation (RMSF) of all bases calculated from the final 100 ns of the simulation time for regular and amphiphilic monomers, respectively. (**D**) RMSF of all bases constituting four inner arms of each structure. Bases near cholesterols generally have lower RMSF values. (**E, F**) Potential of mean force (PMF) between two (**E**) regular and (**F**) amphiphilic DNA units. The 500-ns-long sampled trajectories were used. The global minimum state of free energy was clearly observed between amphiphilic units 1 and 2 and units 3 and 4. (**G**) PMF between two cholesterols in arms 1 and 2 and arms 3 and 4.

cholesterol sites were clearly observed (Figure 5D), indicating that cholesterol interaction stabilizes the monomers and leads to the formation of gelated structures. The interaction between each monomer was further studied by calculating the potential of mean force (PMF) (57) (Figure 5E and F) as $w = -k_B T \log(g(r))$, where $g(r)$ is the radial distribution function between the center of mass of each DNA unit. No clear minimum state of global free energy was observed between regular DNA units, indicating that the monomer units were in a dispersed state (Figure 5E). Meanwhile, the lowest free energy states existed in amphiphilic units 1 and 2 and units 3 and 4, in which two cholesterol-bridged connections were observed (Figure 5B and 5F). Calculation of PMF between two connected cholesterols in arms 1 and 2 and arms 3 and 4 revealed that the inter-cholesterol distance post connection was approximately 6 Å (Figure 5G). Finally, the distribution of sodium and spermine ions near the DNA backbone phosphate was not affected by the presence of cholesterol moieties (Supplementary Figure S18), which supports the experimental finding that regular and amphiphilic DNA units mixed with spermine showed similar aggregation behavior prior to the addition of NaCl.

In summary, we demonstrated the non-conventional isothermal gelation of amphiphilic DNA nanostructures by utilizing their sequential phase transitions. Phase separation of DNA with polyelectrolytes has been attracted since the condensation behavior was common in a biological system (58) and it can be a powerful mechanism for the formation of higher-order DNA assemblies. Electrostatic interactions between DNA and spermine led to the initial phase separation of monomer units to solid aggregates. Based on this electrostatic-driven process, we designed amphiphilic DNA nanostructures for utilizing hydrophobic interaction to connect unit structures. Gelation of condensates was triggered by the addition of NaCl, which weakened the DNA-spermine interaction while cholesterol bonds led to a stable connection between monomers. The shape and viscosity of DNA microgels can be controlled by

the number and design of hydrophobic functional groups in monomers as well as the final NaCl concentration in solution. It was enabled by taking advantage of DNA nanotechnology that the degree of hydrophobicity of a unit structure can be tailored precisely. Since the solid-to-gel transition of amphiphilic condensates can be facially initiated on the desired substrate, *in situ* gelation of DNA assemblies was demonstrated using micropatterned surfaces. We expect that our proposed mechanism can provide insights into new design principles and assembly mechanisms for DNA-based higher-order structures. Our method can be used for gelation of more complex DNA assemblies, including tile- and origami-based DNA nanostructures. Further, a combination of our *in situ* gelation method with conventional top-down fabrication techniques may expand the range of biological and therapeutic applications of DNA hydrogels (19,59).

DATA AVAILABILITY

All data are available in the main text or supplementary information.

SUPPLEMENTARY DATA

Supplementary Data are available at NAR Online.

FUNDING

This research was supported by the National Convergence Research of Scientific Challenges (NRF-2020M3F7A1094299, NRF-2020M3F7A1094300) through the National Research Foundation of Korea (NRF) funded by the Ministry of Science and ICT and by the National Supercomputing Center with supercomputing resources including technical support (KSC-2020-CRE-0042). C. Lee acknowledges the support of the Basic Science Research Program through NRF funded by the Ministry of Education (NRF-2019R1A6A3A01090428, NRF-2020R1A6A3A03037120).
Conflict of interest statement. None declared.

REFERENCES

1. Seeman,N.C. and Sleiman,H.F. (2017) DNA nanotechnology. *Nat. Rev. Mater.*, **3**, 17068.
2. Seeman,N.C. (1982) Nucleic acid junctions and lattices. *J. Theor. Biol.*, **99**, 237–247.
3. Rothemund,P.W.K. (2006) Folding DNA to create nanoscale shapes and patterns. *Nature*, **440**, 297–302.
4. Douglas,S.M., Dietz,H., Liedl,T., Hogberg,B., Graf,F. and Shih,W.M. (2009) Self-assembly of DNA into nanoscale three-dimensional shapes. *Nature*, **459**, 414–418.
5. Yin,P., Hariadi,R.F., Sahu,S., Choi,H.M.T., Park,S.H., LaBean,T.H. and Reif,J.H. (2008) Programming DNA tube circumferences. *Science*, **321**, 824–826.
6. Hong,F., Zhang,F., Liu,Y. and Yan,H. (2017) DNA origami: Scaffolds for creating higher order structures. *Chem. Rev.*, **117**, 12584–12640.
7. Chen,Y., Sun,W., Yang,C. and Zhu,Z. (2020) Scaling up DNA self-assembly. *ACS Appl. Bio Mater.*, **3**, 2805–2815.
8. Gerling,T., Wagenbauer,K.F., Neuner,A.M. and Dietz,H. (2015) Dynamic DNA devices and assemblies formed by shape-complementary, non–base pairing 3D components. *Science*, **347**, 1446–1452.
9. Zheng,J., Birktoft,J.J., Chen,Y., Wang,T., Sha,R., Constantinou,P.E., Ginell,S.L., Mao,C. and Seeman,N.C. (2009) From molecular to macroscopic via the rational design of a self-assembled 3D DNA crystal. *Nature*, **461**, 74–77.
10. Zhang,T., Hartl,C., Frank,K., Heuer-Jungemann,A., Fischer,S., Nickels,P.C., Nickel,B. and Liedl,T. (2018) 3D DNA origami crystals. *Adv. Mater.*, **30**, 1800273.
11. Um,S.H., Lee,J.B., Park,N., Kwon,S.Y., Umbach,C.C. and Luo,D. (2006) Enzyme-catalysed assembly of DNA hydrogel. *Nat. Mater.*, **5**, 797–801.
12. Nguyen,D.T. and Saleh,O.A. (2017) Tuning phase and aging of DNA hydrogels through molecular design. *Soft Matter*, **13**, 5421–5427.
13. Jeon,B., Nguyen,D.T., Abraham,G.R., Conrad,N., Fygenson,D.K. and Saleh,O.A. (2018) Salt-dependent properties of a coacervate-like, self-assembled DNA liquid. *Soft Matter*, **14**, 7009–7015.
14. Zeng,J., Fu,W., Qi,Z., Zhu,Q., He,H., Huang,C., Zuo,H. and Mao,C. (2019) Self-assembly of microparticles by supramolecular homopolymerization of one component DNA molecule. *Small*, **15**, 1805552.
15. Nishikawa,M., Mizuno,Y., Mohri,K., Matsuoka,N., Rattanakiat,S., Takahashi,Y., Funabashi,H., Luo,D. and Takakura,Y. (2011) Biodegradable CpG DNA hydrogels for sustained delivery of doxorubicin and immunostimulatory signals in tumor-bearing mice. *Biomaterials*, **32**, 488–494.
16. Xing,Y., Cheng,E., Yang,Y., Chen,P., Zhang,T., Sun,Y., Yang,Z. and Liu,D. (2011) Self-assembled DNA hydrogels with designable thermal and enzymatic responsiveness. *Adv. Mater.*, **23**, 1117–1121.
17. Bomboi,F., Romano,F., Leo,M., Fernandez-Castanon,J., Cerbino,R., Bellini,T., Bordi,F., Filetici,P. and Sciortino,F. (2016) Re-entrant DNA gels. *Nat. Commun.*, **7**, 13191.
18. Cheng,E., Xing,Y., Chen,P., Yang,Y., Sun,Y., Zhou,D., Xu,L., Fan,Q. and Liu,D. (2009) A pH-triggered, fast-responding DNA hydrogel. *Angew. Chem. Int. Ed.*, **48**, 7660–7663.
19. Jin,J., Xing,Y., Xi,Y., Liu,X., Zhou,T., Ma,X., Yang,Z., Wang,S. and Liu,D. (2013) A triggered DNA hydrogel cover to envelop and release single cells. *Adv. Mater.*, **25**, 4714–4717.
20. Guo,W., Qi,X.-J., Orbach,R., Lu,C.-H., Freage,L., Mironi-Harpaz,I., Seliktar,D., Yang,H.-H. and Willner,I. (2014) Reversible Ag+-crosslinked DNA hydrogels. *Chem. Commun.*, **50**, 4065–4068.
21. Lee,J.B., Peng,S., Yang,D., Roh,Y.H., Funabashi,H., Park,N., Rice,E.J., Chen,L., Long,R., Wu,M. *et al.* (2012) A mechanical metamaterial made from a DNA hydrogel. *Nat. Nanotechnol.*, **7**, 816–820.
22. Merindol,R., Delechiave,G., Heinen,L., Catalani,L.H. and Walther,A. (2019) Modular design of programmable mechanofluorescent DNA hydrogels. *Nat. Commun.*, **10**, 528.
23. Merindol,R., Loescher,S., Samanta,A. and Walther,A. (2018) Pathway-controlled formation of mesostructured all-DNA colloids and superstructures. *Nat. Nanotechnol.*, **13**, 730–738.
24. Sato,Y., Sakamoto,T. and Takinoue,M. (2020) Sequence-based engineering of dynamic functions of micrometer-sized DNA droplets. *Sci. Adv.*, **6**, eaba3471.
25. Jones,M.R., Seeman,N.C. and Mirkin,C.A. (2015) Programmable materials and the nature of the DNA bond. *Science*, **347**, 1260901.
26. Tian,Y., Zhang,Y., Wang,T., Xin,H.L., Li,H. and Gang,O. (2016) Lattice engineering through nanoparticle-DNA frameworks. *Nat. Mater.*, **15**, 654–661.
27. Tang,H., Duan,X., Feng,X., Liu,L., Wang,S., Li,Y. and Zhu,D. (2009) Fluorescent DNA–poly(phenylenevinylene) hybrid hydrogels for monitoring drug release. *Chem. Commun.*, 641–643.
28. Raspaud,E., Olvera de la Cruz,M., Sikorav,J.L. and Livolant,F. (1998) Precipitation of DNA by polyamines: A polyelectrolyte behavior. *Biophys. J.*, **74**, 381–393.
29. Vieregg,J.R., Lueckheide,M., Marciel,A.B., Leon,L., Bologna,A.J., Rivera,J.R. and Tirrell,M.V. (2018) Oligonucleotide–peptide complexes: Phase control by hybridization. *J. Am. Chem. Soc.*, **140**, 1632–1638.
30. Bloomfield,V.A. (1996) DNA condensation. *Curr. Opin. Struct. Biol.*, **6**, 334–341.
31. Pardatscher,G., Bracha,D., Daube,S.S., Vonshak,O., Simmel,F.C. and Bar-Ziv,R.H. (2016) DNA condensation in one dimension. *Nat. Nanotechnol.*, **11**, 1076–1081.

32. Shakya,A. and King,J.T. (2018) DNA local-flexibility-dependent assembly of phase-separated liquid droplets. *Biophys. J.*, **115**, 1840–1847.
33. Hyde,A.M., Zultanski,S.L., Waldman,J.H., Zhong,Y.-L., Shevlin,M. and Peng,F. (2017) General principles and strategies for salting-out informed by the Hofmeister series. *Org. Process Res. Dev.*, **21**, 1355–1370.
34. Zangi,R., Hagen,M. and Berne,B.J. (2007) Effect of ions on the hydrophobic interaction between two plates. *J. Am. Chem. Soc.*, **129**, 4678–4686.
35. Lee,C., Kim,S.M., Kim,Y.J., Choi,Y.W., Suh,K.-Y., Pang,C. and Choi,M. (2015) Robust microzip fastener: Repeatable interlocking using polymeric rectangular parallelepiped arrays. *ACS Appl. Mater. Interfaces*, **7**, 2561–2568.
36. Douglas,S.M., Marblestone,A.H., Teerapittayanon,S., Vazquez,A., Church,G.M. and Shih,W.M. (2009) Rapid prototyping of 3D DNA-origami shapes with cadnano. *Nucleic Acids Res.*, **37**, 5001–5006.
37. Lee,J.Y., Lee,J.G., Yun,G., Lee,C., Kim,Y.-J., Kim,K.S., Kim,T.H. and Kim,D.-N. (2021) Rapid computational analysis of DNA origami assemblies at near-atomic resolution. *ACS Nano*, **15**, 1002–1015.
38. Vanommeslaeghe,K., Hatcher,E., Acharya,C., Kundu,S., Zhong,S., Shim,J., Darian,E., Guvench,O., Lopes,P., Vorobyov,I. *et al.* (2010) CHARMM general force field: A force field for drug-like molecules compatible with the CHARMM all-atom additive biological force fields. *J. Comput. Chem.*, **31**, 671–690.
39. Jo,S., Kim,T., Iyer,V.G. and Im,W. (2008) CHARMM-gui: A web-based graphical user interface for CHARMM. *J. Comput. Chem.*, **29**, 1859–1865.
40. Yoo,J. and Aksimentiev,A. (2016) Improved parameterization of amine–carboxylate and amine–phosphate interactions for molecular dynamics simulations using the CHARMM and AMBER force fields. *J. Chem. Theory Comput.*, **12**, 430–443.
41. Humphrey,W., Dalke,A. and Schulten,K. (1996) VMD: Visual molecular dynamics. *J. Mol. Graph.*, **14**, 33–38.
42. Phillips,J.C., Braun,R., Wang,W., Gumbart,J., Tajkhorshid,E., Villa,E., Chipot,C., Skeel,R.D., Kalé,L. and Schulten,K. (2005) Scalable molecular dynamics with NAMD. *J. Comput. Chem.*, **26**, 1781–1802.
43. Feller,S.E., Zhang,Y., Pastor,R.W. and Brooks,B.R. (1995) Constant pressure molecular dynamics simulation: The Langevin piston method. *J. Chem. Phys.*, **103**, 4613–4621.
44. Hart,K., Foloppe,N., Baker,C.M., Denning,E.J., Nilsson,L. and MacKerell,A.D. (2012) Optimization of the CHARMM additive force field for DNA: Improved treatment of the BI/BII conformational equilibrium. *J. Chem. Theory Comput.*, **8**, 348–362.
45. Yoo,J. and Aksimentiev,A. (2012) Improved parametrization of Li+, Na+, K+, and Mg2+ ions for all-atom molecular dynamics simulations of nucleic acid systems. *J. Phys. Chem. Lett.*, **3**, 45–50.
46. Miyamoto,S. and Kollman,P.A. (1992) Settle: An analytical version of the SHAKE and RATTLE algorithm for rigid water models. *J. Comput. Chem.*, **13**, 952–962.
47. Andersen,H.C. (1983) Rattle: A "velocity" version of the shake algorithm for molecular dynamics calculations. *J. Comput. Phys.*, **52**, 24–34.
48. Essmann,U., Perera,L., Berkowitz,M.L., Darden,T., Lee,H. and Pedersen,L.G. (1995) A smooth particle mesh ewald method. *J. Chem. Phys.*, **103**, 8577–8593.
49. Ohmann,A., Göpfrich,K., Joshi,H., Thompson,R.F., Sobota,D., Ranson,N.A., Aksimentiev,A. and Keyser,U.F. (2019) Controlling aggregation of cholesterol-modified DNA nanostructures. *Nucleic Acids Res.*, **47**, 11441–11451.
50. Zhang,Y., Peng,R., Xu,F. and Ke,Y. (2019) Hierarchical self-assembly of cholesterol-DNA nanorods. *Bioconjugate Chem.*, **30**, 1845–1849.
51. Jain,A. and Vale,R.D. (2017) RNA phase transitions in repeat expansion disorders. *Nature*, **546**, 243–247.
52. List,J., Weber,M. and Simmel,F.C. (2014) Hydrophobic actuation of a DNA origami bilayer structure. *Angew. Chem. Int. Ed.*, **53**, 4236–4239.
53. Shimomura,S., Nishimura,T., Ogura,Y. and Tanida,J. (2018) Photothermal fabrication of microscale patterned DNA hydrogels. *R. Soc. Open Sci.*, **5**, 171779.
54. Kasahara,Y., Sato,Y., Masukawa,M.K., Okuda,Y. and Takinoue,M. (2020) Photolithographic shape control of DNA hydrogels by photo-activated self-assembly of DNA nanostructures. *APL Bioengineering*, **4**, 016109.
55. Wang,J., Chao,J., Liu,H., Su,S., Wang,L., Huang,W., Willner,I. and Fan,C. (2017) Clamped hybridization chain reactions for the self-assembly of patterned DNA hydrogels. *Angew. Chem. Int. Ed.*, **56**, 2171–2175.
56. Lee,T., Do,S., Lee,J.G., Kim,D.-N. and Shin,Y. (2021) The flexibilitybased modulation of DNA nanostar phase separation. *Nanoscale*, **13**, 17638–17647.
57. Chandler,D. (1987) In: *Introduction to Modern Statistical Mechanics*. Oxford University Press, Oxford, UK, Vol. **5**.
58. Shin,Y. (2022) Rich phase separation behavior of biomolecules. *Mol. Cells*, **45**, 6–15.
59. Jiang,Q., Zhao,S., Liu,J., Song,L., Wang,Z.-G. and Ding,B. (2019) Rationally designed DNA-based nanocarriers. *Adv. Drug Deliv. Rev.*, **147**, 2–21.